Elucidating the Electronic Structure of the Ligated Cuboctahedral Palladium Cluster [Pd13(μ4-C7H7)6]2+

Jianyu Wei, Samia Kahlal, Jean-François Halet, Jean-Yves Saillard

Elucidating the Electronic Structure of the Ligated Cuboctahedral Palladium Cluster $[Pd_{13}(\mu_4\text{-}C_7H_7)_6]^{2+}$

Jianyu Wei, Samia Kahlal, Jean-François Halet,* and Jean-Yves Saillard*

Univ Rennes, CNRS, Institut des Sciences Chimiques de Rennes (ISCR) – UMR 6226, F-35000 Rennes, France

Abstract The electronic structure of the recently reported cuboctahedral $[Pd_{13}(\mu_4\text{-}Tr)_6]^{2+}$ (Tr = C_7H_7) cluster is analyzed using DFT calculations. Results indicate that the bonding in this cluster can be described from the formal starting point of a $[Pd_{13}]^{2-}$ core interacting with a partly reduced $[Tr_6]^{4+}$ ligand shell. The orbital interactions between the two fragments are strong, owing in particular to the very strong accepting ability of the surrounding ligands. The (moderate) Pd-Pd bonding character is in part due to the occupation of the strongly bonding in-phase combination of the *5s*(Pd) orbitals (the 1S jellium level) and for another part from through-bond interactions.

Electronic supplementary material The online version of this article (doi:xx) contains supplementary material, which is available to authorized users.

* Corresponding authors. E-mail: halet@univ-rennes1.fr (J.-F. H.) and saillard@univ-rennes1.fr (J.-Y. S.)

Introduction

In 1869 Mendeleev published his Periodic Table [1]. Discovered in 1803, palladium element is then mentioned among the 60 elements reported in the table. 150 years later, in the International Year of the Periodic Table of the Elements, palladium is a key chemical element largely used in catalysis but also in electronics, dentistry, medicine, hydrogen purification, chemical applications, groundwater treatment, jewelry, etc. Over the last decades, it became apparent that palladium in its zero-valent state, forms unique highly condensed nano-sized carbonyl-ligated clusters [2, 3], distinguishing itself from other elements, including the other two Group 10 congeneric Ni and Pt metals [4-6] Indeed, relatively weak metal–metal and metal–carbonyl (and/or phosphine) connectivity must be responsible for the rich variety of structural arrangements reported for these high-nuclearity ligated clusters, which can extend up to 165 atoms (so far) [7]. A substantial number of them have been crystallographically identified [3], and theoretically investigated [8-10]. Interestingly, they adopt various shapes, ranging from ‘‘bulk-like’’ cubic closed packed and/or hexagonal closed packed architectures to, also compact but “molecular” icosahedral shapes. Surprisingly, the bonding properties of these ligated Group 10 metal clusters do not parallel those of the coinage metal Cu, Ag or Au ligated clusters. Whereas the cluster architecture of the latter species can generally be rationalized within the *superatom* paradigm based on the spherical *jellium* model [9, 11-18] that of palladium still lacks general rationalization rules.

Ligands certainly play an important role in stabilizing the metallic cluster cores of these species. Despite similar bonding properties of σ-donating CO and phosphine ligands with cyclic hydrocarbon ligands [19], palladium clusters ligated with the latter are very scarce. The fascinating compound recently synthesized and characterized by Teramoto *et al.*, namely $[Pd_{13}(\mu_4\text{-}Tr)_6][B(Ar^F)_4]_2$ ($Tr = C_7H_7$, $Ar^F = 3,5\text{-}(CF_3)_2C_6H_3$) constitutes one example [20]. Its uniqueness comes not only from the nature of the fairly “exotic” cyclic hydrocarbon tropylium ligands (formally $C_7H_7^+$), but also from the structural arrangement of its Pd_{13} core (Figure 1). Indeed, contrarily to many M_{13} clusters which adopt either a centered icosahedral arrangement [21-26] or a centered anticuboctahedral geometry [27-29], the metal atoms in $[Pd_{13}Tr_6]^{2+}$ are forming a centered cuboctahedron, a scarcely encountered architecture in transition-metal chemistry [30, 31] (Scheme 1). Indeed, although the centered cuboctahedron can be seen as a

chunk of face centered cubic bulk metal, it is less compact than the M_{13} centered icosahedron. On the other hand, a cuboctahedral core provides to the tropylium ligands with six size-adapted square faces to cap. Its electron count, 170 cluster valence electrons (cve) if the Tr^{+} ligands are assumed to give 6 electrons to the cluster, is also puzzling, since, assuming cationic tropylium ligands, the resulting putative $[Pd_{13}]^{4-}$ core is in a negative oxidation state. This is in contrast with the Pd^{0} oxidation state found ordinarily in the carbonyl- or phosphine-protected clusters [3]. In fact, we will show below that the metal core is best described, as in a formal $[Pd_{13}]^{2-}$ state, at least in a starting point, before considering interaction with the ligand shell. Interestingly also, 170 cve is also the electron count for the anticuboctahedral cluster $[H_2Rh_{13}(CO)_{24}]^{3-}$ [27-29], or for the icosahedral species $[Rh_{12}(\mu\text{-}_{12}S)CO]_{27}]^{3-}$ [32, 33], for instance. All these three structures share a common valence electron count obeying the $14n_s$ + 2 cve rule proposed by Mingos for spherical high nuclearity ligated clusters [34-36], despite a different number of triangular and square faces (Scheme 1).

Scheme 1 Different twelve-vertex geometrical isomeric cluster cores : a) cuboctahedral, b) icosahedral, and c) anticuboctahedral

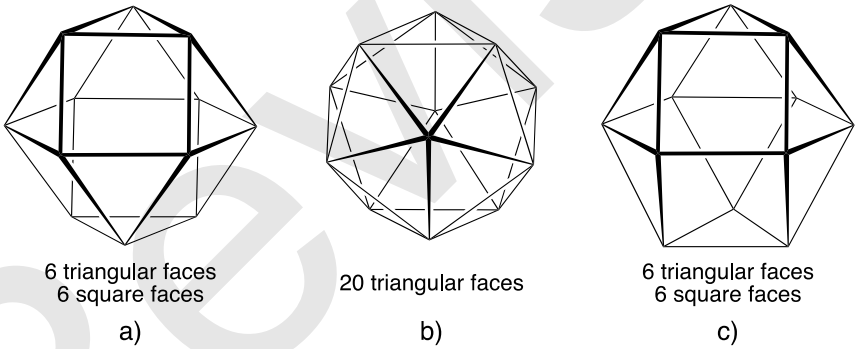

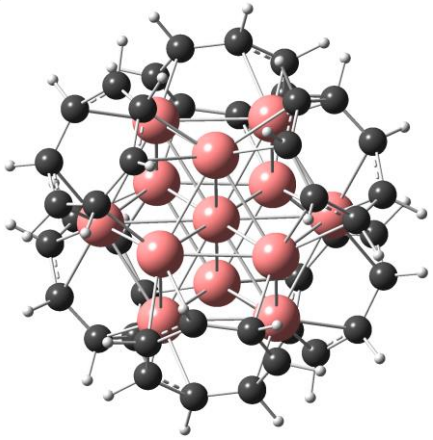

Fig. 1 The molecular structure of $[Pd_{13}(\mu_4\text{-}C_7H_7^{+})_6]^{2+}$ characterized by Teramoto *et al.* [20]

Although Moller-Plesset (MP2) computations on $[Pd_{13}(\mu_4\text{-}Tr)_6]^{2+}$ were reported by Teramoto *et al.* [20], no detailed rationalization of its peculiar structure on the basis of its valence electron count has been provided yet. This prompted us to undertake a detailed analysis of its electronic structure by means of density functional theory (DFT) calculations, in order to provide an orbital interpretation of its bonding, structure and stability. The main results are discussed here.

Computational Details

Geometry optimizations were carried out with the Gaussian 09 package [37] at the DFT level of theory. The BP86 functional [38, 39] and the general triple-ξ-polarized Def2-TZVP basis set were used to perform all-electron calculations. The optimized geometries were characterized as true minima on their potential energy surface by harmonic vibrational analysis. Wiberg indices and natural orbital populations analyses were computed by using NBO 5.0 program [40]. The compositions of the molecular orbitals were calculated with the AOMix Program [41] The bonding analysis was performed by carrying out a fragment decomposition analysis with the help of the ADF2016 program [42], using the BP86 functional [38, 39] and an STO all-electron TZP basis set [43]. This fragment decomposition analysis was based on single-point calculations using the Gaussian-optimized geometries.

During the evaluation process of this manuscript, one of the reviewers asked for considering dispersion forces by including Grimme's empirical DFT-D3 corrections [44]. Therefore, the Gaussian 09 and ADF2016 calculations described above were then performed with inclusion of such corrections. Except for leading to somewhat shorter Pd-Pd optimized bond distances (see below), the results obtained with and without dispersion corrections are very much the same, as exemplified by the major computed data obtained with DFT-D3 corrections (Table S1) which can be compared with those given in Table 1 below.

Results and Discussion

The optimized structure of $[Pd_{13}Tr_6]^{2+}$ was found to be of C_{2h} symmetry, the C_2 axis passing through two opposite vertices. A similar optimized geometry was found at the MP2 level of theory [20]. Its Kohn-Sham molecular orbital (MO) diagram is shown in Fig. 2. The reasonably large HOMO-LUMO gap computed at the GGA level of theory (0.72 eV) is

consistent with the cluster stability and experimental diamagnetic behavior. The two lowest unoccupied orbitals (LUMO) are similar to those shown by Teramoto *et al.* [20], being evenly distributed on the metallic core and the ligand shell. On the other hand, the highest occupied orbitals (HOMO) are mostly localized on the cuboctahedral Pd_{12} core and to a lesser extent on the ligand envelope. They hardly show any character on the interstitial Pd atom.

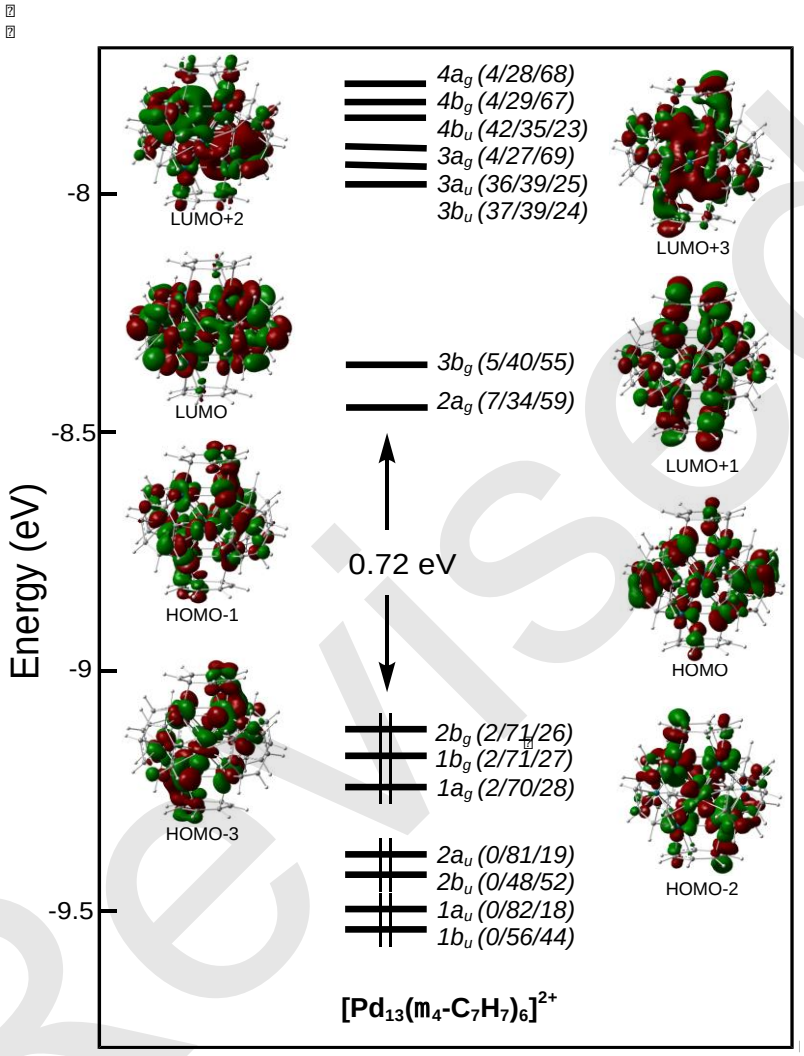

Fig. 2 Kohn-Sham orbital diagram of the $[Pd_{13}Tr_6]^{2+}$ cluster (C_{2h} symmetry). Values in parentheses are the orbital localization (in %) on the interstitial Pd atom, Pd_{12} cuboctahedral core and Tr_6 ligand shell, respectively

The major computed metrical data are given in Table 1, together with their corresponding experimental ones [20]. The optimized Pd-Pd distances are ~ 3% larger than those measured experimentally, as often found for late transition-metal-containing molecules using with GGA functionals. Inclusion of Grimme's D3 corrections [44] reduces this difference to ~ 1% (see Table S1). As a whole however, the agreement between the optimized and X-ray

structure is fairly good. The metal cuboctahedron does not depart importantly from the ideal O_h symmetry. The computed Pd-Pd Wiberg indices (avg. 0.095) are indicative of moderate metal-metal bonding interactions. The natural atomic orbital (NAO) charges (Table 1) correspond to $[Pd_{13}]^{+3.80}$ and $[Tr_6]^{-1.80}$, indicating significant electron transfer from the metal core to the tropylium ligands. As expected, the interstitial Pd atom (Pd_i, charge = -0.70) is largely more electron-rich than the peripheral metal atoms (average charge = + 0.38). The charge distribution on the Pd atoms and Tr ligands is consistent with a pseudo-O_h symmetry of the whole cluster.

Table 1 Relevant computed data for $[Pd_{13}Tr_6]^{2+}$. Interatomic distances are given in Å. The corresponding Wiberg indices are given in brackets. Experimental bond distances are also given for comparison

		$[Pd_{13}Tr_6]^{2+}$
HOMO-LUMO gap (eV)		0.72 eV
Pd_i-Pd_{cubo}		4 x 2.808 [0.109] 2 x 2.808 [0.107] 4 x 2.793 [0.111] 2 x 2.813 [0.108] Avg: 2.804 [0.1090] (exp: 2.720)
Pd_{cubo}-Pd_{cubo}		2 x 2.900 [0.071] 2 x 2.718 [0.102] 4 x 2.808 [0.082] 4 x 2.770 [0.089] 4 x 2.835 [0.078] 4 x 2.749 [0.096] 4 x 2.856 [0.076] Avg: 2.808 [0.085] (exp. 2.720)
Pd_{cubo}-C		Range: 2.189-2.556 (exp: 2.084-2.607) Avg: 2.300 [0.191] (exp: 2.302)
NAO charges	Pd_i	-0.695
	Pd_{cubo}	4 x 0.377 4 x 0.378 2 x 0.356 2 x 0.384
	Tr	2 x -0.307 4 x -0.297

In order to get a deeper understanding of the electronic structure of $[Pd_{13}Tr_6]^{2-}$, with the help of the ADF program (see computational details), its molecular one-electron orbitals were expressed as linear combinations of the orbitals of two fragments (assumed to be in singlet states), namely the metal Pd_{13} core and the Tr_6 octahedral envelope. Then, the question of fragment charge partitioning arises. The tropylium ligand being known to be stable in its

aromatic cationic form, the *a priori* most obvious fragmentation is $[Pd_{13}]^{4-}$ and $[Tr_6]^{6+}$. Unfortunately, the $[Pd_{13}]^{4-}$ fragment could not be converged in a singlet ground state, but rather in an "excited" singlet state. A singlet ground state could be obtained only for a neutral $[Pd_{13}]^0$ fragment, but on the other hand, the $[Tr_6]^{2+}$ counterpart converged in an excited singlet state. Obviously, regardless of the charge partitioning, a Kohn-Sham description of the two fragments in singlet ground states appears to be only approximate. However, independently of the charge partitioning, the qualitative description of the bonding picture, which arises from a fragment analysis is the same. In particular, the occupations of the fragment orbitals in the whole cluster are rather stable with respect to the choice of fragment charges. The values discussed below correspond to $[Pd_{13}]^0$ and $[Tr_6]^{2+}$. The qualitative interaction MO diagram is shown below, but before investigating it in detail, we would like to first analyze the electronic structure of a centered cuboctahedral $[Pd_{13}]$ bare cluster. This should indirectly provide us some information about the role of the ‘‘protective’’ ligand environment

Fig. 3 illustrates the Kohn-Sham orbital diagram obtained by a single-point calculation on a regular $[Pd_{13}]^0$ species of O_h symmetry (Pd-Pd = 2.80 Å). The 13 x 5 = 65 weakly bonding/antibonding combinations of the *4d*(Pd) atomic orbitals (AO) constitute the so-called *d*-block. However, the more antibonding one, of a_{1u} symmetry, lies slightly above the other 64 closely energetically spaced combinations and is unoccupied (see Fig. 2). Because of substantial overlap, the *5s*(Pd) combinations split within a huge range of energy. In particular, the in-phase combination (a_{1g}) is so importantly stabilized that it lies just below the *d*-block bottom. Within the spherical jellium model, this level is associated with the 1S superatomic orbital. The next *5s*(Pd) bonding combinations are of t_{1u} symmetry and correspond to the 1P superatomic shell. They are situated just below the highest a_{1u} *4d*(Pd) level. The next *5s*(Pd) combinations (1D and 2S superatomic levels) lie above this a_{1u} orbital. Above them, one finds the lowest combination of dominant *5p*(Pd) character, which is of a_{2u} symmetry. Owing to its small HOMO-LUMO gap, such a neutral cuboctahedral architecture is not a stable species.

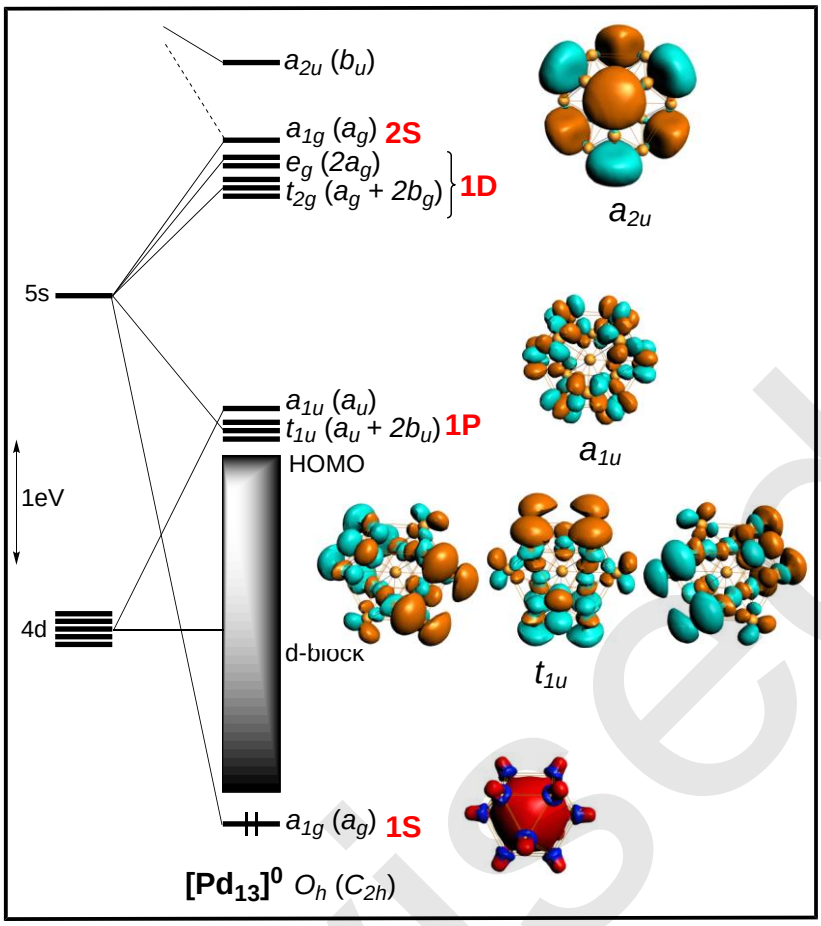

Fig. 3 Kohn-Sham orbital diagram of a neutral centered cuboctahedral [Pd_{13}] unit of O_h symmetry. The irreducible representations expressed in C_{2h} symmetry are given in parenthesis

The qualitative MO diagram of $[Pd_{13}Tr_6]^{2+}$ built as the result of the interaction between the metal core and its ligand envelope is sketched in Fig. 4. The charge distribution $[Pd_{13}]^{2-}$ and $[Tr_6]^{4+}$ was assumed (see below for its justification). Owing to the fact that the cluster symmetry does not depart that much from the ideal O_h symmetry, the orbital diagram of the Pd_{13} fragment (left side of Fig. 4) is not very different from that shown in Fig. 3. Its orbitals are labeled in the actual C_{2h} cluster symmetry (see Fig. 3). The π MO level energy ordering of an isolated tropylium ion of D_{7h} symmetry (far right-hand side of Fig. 4) is $a''_2 < e''_1 < e''_2 < e''_3$, of which a''_2 and e''_1 are bonding and contain the six π-electrons of Tr^+. Owing to the electrophilic character of the ligand, its antibonding e''_2 LUMOs are rather low-lying in energy. In the pseudo-octahedral Tr_6 fragment, each individual Tr orbital generates six combinations. The occupied π-combinations are somewhat stabilized by vacant *5s*/*5p*(Pd) combinations of the Pd_{13} fragment, including the t_{1u} (1P) level, which is in turn destabilized. The corresponding ligand-to-metal electron donation is ~1.6 e. On the other hand, the π* Tr_6 combinations interact

importantly with occupied *4d*(Pd) levels, in particular those deriving from the e''_2 level. However, one of these combinations of b_u symmetry behaves differently. Indeed, it interacts particularly strongly with the vacant b_u *5p*(Pd) level labeled a_{2u} (O_h symmetry) in Fig. 3, in such a way it generates a bonding combination, which is sufficiently low-lying in energy to be occupied in the cluster. The occupation in $[Pd_{13}Tr_6]^{2+}$ of this e''_2-derived b_u fragment orbital is 1.7 e. This indicates that, from the point of view of oxidation states, it is formally occupied. Thus, the ligand fragment, being formally $[Tr_6]^{4+}$, is reduced by the metal core. The metal-to-ligand electron-transfer involving all the other formally vacant ligand π* combinations is also substantial, ~7.1 e, and concerns mainly the 11 formally vacant e''_2 combinations. This very large electron transfer is the footprint of the substantial metal-ligand mixing in the orbitals shown in Fig. 2.

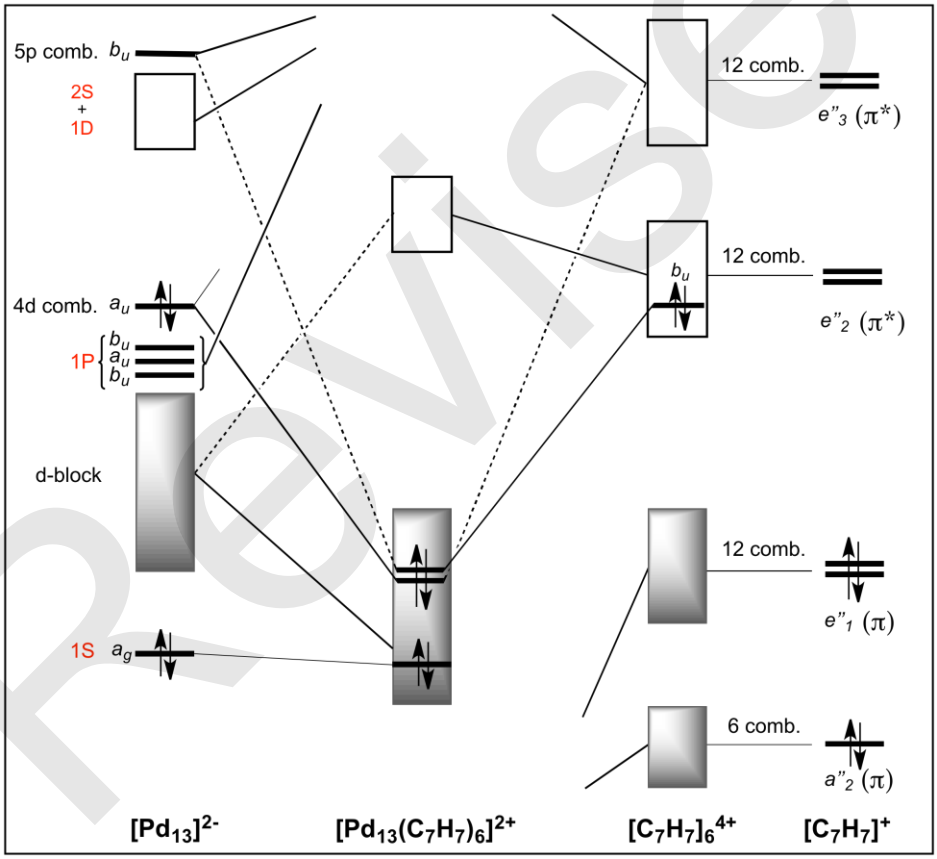

Fig. 4 Qualitative MO diagram illustrating the interaction between the centered cubocathedral cage $[Pd_{13}]^{2-}$ and the $[Tr_6]^{4+}$ ligand envelope in $[Pd_{13}Tr_6]^{2+}$ of C_{2h} symmetry

Assuming the charged $[Tr_6]^{4+}$ fragment implies an anionic $[Pd_{13}]^{2-}$ core. Actually, all the *4d*(Pd) levels are formally occupied in $[Pd_{13}Tr_6]^{2+}$, including the highest a_u combination. Indeed, this orbital interacts strongly with ligand π*(a_u) combinations and is in turn stabilized

below the HOMO after interaction (occupation 1.8 e). Thus, the full *d*-block is occupied in the complex, as well as the additional strongly bonding jellium 1S level (in-phase combination of the *5s*(Pd) AOs), which is responsible for a large part of the Pd-Pd bonding character in $[Pd_{13}Tr_6]^{2+}$. Another significant contribution to Pd-Pd bonding comes from the mixing of the metal-metal bonding orbitals (1P and a_u(*5p*), occupations 1.3 and 0.3 e, respectively) into occupied levels through their mixing with ligand orbitals.

Cyclic voltammetry experiments of $[Pd_{13}Tr_6]^{2+}$ indicated two reversible one-electron oxidations and one reversible one-electron reduction [20]. The paramagnetic tricationic cluster was chemically prepared and X-ray characterized. Our calculations indicate that the one-electron oxidation of $[Pd_{13}Tr_6]^{2+}$ corresponds to an electron removal from the HOMO (see Figure S1, Supplementary information), without any significant structural change (see Table T1, Supplementary information). The spin density of $[Pd_{13}Tr_6]^{3+}$ is concentrated on the metal core (see Figure S2, Supplementary information), thus allowing kinetic protection from the ligand shell envelope. Calculations on the monoreduced species $[Pd_{13}Tr_6]^{2+}$ indicate occupation of the LUMO (see Figure S3, Supplementary information), again without little structural change (see Table S2, Supplementary information).

Concluding Remarks

The bonding in the cluster $[Pd_{13}Tr_6]^{2+}$ can be formally from the starting point of a $[Pd_{13}]^{2-}$ core interacting with partly reduced $[Tr_6]^{4+}$ ligand shell. The orbital interactions between the two fragments are strong, owing in particular to the strong π-accepting ability of the ligands. Consequently, a very important charge transfer occurs between the two fragments, from several d-type combinations of $[Pd_{13}]^{2-}$ to the vacant π* ligand orbitals. Although the formal occupation (2 or 0) of the involved fragment orbitals does not change (no orbital-to-orbital electron transfer larger than 1.0 e), this electron transfer in fact reverses completely the fragment charge polarity. It follows that, in the full $[Pd_{13}Tr_6]^{2+}$ cluster, the Pd_{13} core has an electron configuration corresponding to the formal occupation of all its 4d combinations, plus the in-phase combination of the *5s*(Pd) orbitals (the 1S jellium level). The (moderate) Pd-Pd covalent bonding character is in part due to the occupation of this strongly bonding 1S orbital and for another part from through-bond interactions, in particular from the partial occupation of other bonding *5s*/*5p*(Pd) combinations (of t_{1u} (1P level) and a_{2u} symmetry).

A question which arises from the above discussion is why the $[Pd_{13}Tr_6]^{4+}$ tetracation, formally made of $[Pd_{13}]^{2-}$ and six aromatic $(C_7H_7)^+$ ligands was not isolated? Our calculations on $[Pd_{13}Tr_6]^{4+}$ found a very small HOMO($1b_g$)-LUMO($2b_g$) gap of 0.24 eV for the singlet ground state (major computed data in the SI). Thus, the tetracation is likely not to be stable. Moreover, the expected electron configurations for the tetracation should be that which corresponds to the depopulation of a ligand-based b_u level from the parent dianion, restoring full aromaticity to the ligands. One of the possible reasons for such a situation could be the particularly large electrophilicity of tropylium beside of the (relative) basicity of the palladium core.

The peculiar centered cuboctahedral architecture is probably favored, as originally suggested by Teramoto *et al.*, [20] by the size of the tropylium ligands, which are particularly suited for capping Pd_4 square faces. It is noteworthy that centered cuboctahedral copper clusters of the type $[Cu_{13}\{S_2CNR_2\}_6(CCR')_4]^+$ have also been suggested to be stabilized because of the preference of the dithiocarbamate ligands to cap square faces [30, 45]. Interestingly, such copper species are also 2-electron superatomic species with $1S^2$ jellium configuration. However, the comparison between palladium clusters such as $[Pd_{13}Tr_6]^{2+}$ and superatomic clusters of Group 11 metals should not be pushed too far. Indeed, they usually have different electron counts and moreover, contrarily to a large number of Au and Ag clusters, their metal cores do not retain their closed-shell superatom electron configuration when their ligands are removed.

Acknowledgments J.W. thanks the China Scholarship Council for a PhD scholarship. The authors are grateful to GENCI (Grand Equipment National de Calcul Intensif) for HPC resources (grant A0050807367).

References

1. D. Mendeleev (1869). *Z. Chem.* **12**, 405-406.
2. E. G. Mednikov and L. F. Dahl (2009). *J. Chem. Educ.* **86**, 1135-1135.
3. E. G. Mednikov and L. F. Dahl (2010). *Philos. Trans. R. Soc. A* **368**, 1301-1332.
4. O. Belyakova and Y. Slovokhotov (2003). *Russ. Chem. Bull.* **52**, 2299-2327.
5. C. Femoni, M. C. Iapalucci, F. Kaswalder, G. Longoni, and S. Zacchini (2006). *Coord. Chem. Rev.* **250**, 1580-1640.

6. I. Ciabatti, C. Femoni, M. C. Iapalucci, G. Longoni, and S. Zacchini (2014). *J. Clust. Sci.* **25**, 115-146.
7. E. G. Mednikov, M. C. Jewell, and L. F. Dahl (2007). *J. Am. Chem. Soc.* **129**, 11619-11630.
8. R. Marchal, G. Manca, E. Furet, S. Kahlal, J.-Y. Saillard, and J.-F. Halet (2015). *J. Cluster Sci.* **26**, 41-51.
9. J.-Y. Saillard and J.-F. Halet (2016). *Struct. Bond.* **169**, 157-179.
10. G. Frapper and J.-F. Halet in *Computational Materials Discovery* (A. R. Oganov, A. G. Kvashnin, G. Saleh, eds.), Royal Society of Chemistry, London, 2019, pp. 320-351.
11. W. D. Knight, K. Clemenger, W. A. de Heer, W. A. Saunders, M. Y. Chou, and M. L. Cohen (1984) *Phys. Rev. Lett.* **52**, 2141–2143.
12. Z. Lin, T. Slee, and D. M. P. Mingos (1990) *J. Chem. Phys.* **142**, 321-334.
13. W. A. de Heer (1993) *Rev. Mod. Phys.* **65**, 611-676.
14. D. M. P. Mingos in *Structural and Electronic Paradigms in Cluster Chemistry*; Springer; Berlin, Heidelberg, 1997.
15. P. Jena, S. N. Khanna , and B. K. Rao in *Clusters and Nano-Assemblies: Physical and Biological Systems*, World Scientific, 2005.
16. S. N. Khanna and P Jena (2008) *Phys. Rev. Lett*. **51**, 13705-13716.
17. H. Häkkinen (2008). *Chem. Soc. Rev.* **37,** 1847-1859.
18. M. Walter, J. Akola, O. Lopez-Acevedo, P. D. Jadzinsky, G. Calero, C. J. Ackerson, R. L. Whetten, H. Grönbeck, and H. Häkkinen (2008) *Proc. Natl. Acad. Sci. USA* **105**, 9157-9162.
19. M. Elian, M. M.-L. Chen, D. M. P. Mingos, and R. Hoffmann (1976). *Inorg. Chem.* **15**, 1148-1155.
20. M. Teramoto, K. Iwata, H. Yamaura, K. Kurashima, K. Miyazawa, Y. Kurashige, K. Yamamoto, and T. Murahashi (2018). *J. Am. Chem. Soc.* **140**, 12682-12686.
21. C. E. Briant, B. R. C. Theobald, J. W. White, L. K. Bell, D. M. P. Mingos, and A. J. Welch (1981). *J. Chem. Soc., Chem. Commun.* 201-202.
22. M. W. Heaven, A. Dass, P. S. White, K. M. Holt, and R. W. Murray (2008). *J. Am. Chem. Soc.* **130**, 3754-3755.
23. M. Zhu, C. M. Aikens, F. J. Hollander, G. C. Schatz, and R. Jin (2008). *J. Am. Chem. Soc.* **130**, 5883-5885.
24. Y. Negishi, K. Nobusada, and T. Tsukuda (2005). *J. Am. Chem. Soc.* **127**, 5261-5270.

25. C. Femoni, M. C. Iapalucci, G. Longoni, S. Zacchini, and S. Zarra (2011). *J. Am. Chem. Soc.* **133**, 2406-2409.
26. I. Ciabatti, C. Femoni, M. C. Iapalucci, G. Longoni, S. Zacchini, and S. Zarra (2012). *Nanoscale* **4**, 4166-4177.
27. V. G. Albano, A. Ceriotti, P. Chini, G. Ciani, S. Martinengo, and W. M. Anker (1975). *J. Chem. Soc., Chem. Commun.* 859-860.
28. R. Bau, M. H. Drabnis, L. Garlaschelli, W. T. Klooster, Z. Xie, T. F. Koetzle, and S. Martinengo (1997). *Science* **275,** 1099-1102.
29. R. Gautier and J.-F. Halet (1998). *J. Organomet. Chem.* **565,** 217-224.
30. R. P. B. Silalahi, K. K. Chakrahai, J.-H. Liao, S. Kahlal, Y.-C. Liu, M.-H. Chiang, J.-Y. Saillard and C. W. Liu (2018). *Chem. Asian J.* **13**, 500-504.
31. S. Kahlal, C.-W. Liu and J.-Y. Saillard (2017). *Inorg. Chem.* **56**, 1209-1215.
32. J. L. Vidal (1981). *J. Organomet. Chem.* **213**, 351-363.
33. C. Femoni, I. Ciabatti, M. C. Iapalucci, S. Ruggieri, and S. Zacchini (2016). *Prog. Nat. Sci.: Mater. Inter.* **26**, 461-428.
34. D. M. P. Mingos (1985). *J. Chem. Soc. Chem. Commun.* 1352-1354.
35. R. L. Johnston and D. M. P. Mingos (1985). *J. Organomet. Chem.* **280,** 419-428.
36. R. L. Johnston and D. M. P. Mingos (1987). *Struc. Bond.* **68,** 29-87.
37. Gaussian 09, Revision A.1, M. J. Frisch, G. W. Trucks, H. B. Schlegel, G. E. Scuseria, M. A. Robb, J. R. Cheeseman, G. Scalmani, V. Barone, B. Mennucci, G. A. Petersson, H. Nakatsuji, M. Caricato, X. Li, H. P. Hratchian, A. F. Izmaylov, J. Bloino, G. Zheng, J. L. Sonnenberg, M. Hada, M. Ehara, K. Toyota, R. Fukuda, J. Hasegawa, M. Ishida, T. Nakajima, Y. Honda, O. Kitao, H. Nakai, T. Vreven, J. A. Montgomery, Jr., J. E. Peralta, F. Ogliaro, M. Bearpark, J. J. Heyd, E. Brothers, K. N. Kudin, V. N. Staroverov, R. Kobayashi, J. Normand, K. Raghavachari, A. Rendell, J. C. Burant, S. S. Iyengar, J. Tomasi, M. Cossi, N. Rega, J. M. Millam, M. Klene, J. E. Knox, J. B. Cross, V. Bakken, C. Adamo, J. Jaramillo, R. Gomperts, R. E. Stratmann, O. Yazyev, A. J. Austin, R. Cammi, C. Pomelli, J. W. Ochterski, R. L. Martin, K. Morokuma, V. G. Zakrzewski, G. A. Voth, P. Salvador, J. J. Dannenberg, S. Dapprich, A. D. Daniels, O¨ . Farkas, J. B. Foresman, J. V. Ortiz, J. Cioslowski, and D. J. Fox (Gaussian, Inc., Wallingford CT, 2009M).
38. A. D. Becke (1988). *Phys. Rev. A* **38,** 3098-3100.
39. J. P. Perdew (1986). *Phys. Rev. B* **33,** 8822-8824.

40. E. D. Glendening, J. K. Badenhoop, A. E. Reed, J. E. Carpenter, J. A. Bohmann, C. M. Morales, and F. Weinhold, NBO 5.0; Theoretical Chemistry Institute, University of Wisconsin (Madison, WI, 2001, http://www.chem.wisc.edu/nbo5).
41. S. I. Gorelsky. AOMix program; http://www.sg-chem.net.
42. a) G. te Velde, F. M. Bickelhaupt, S. J. A. van Gisbergen, C. Fonseca Guerra, E. J. Baerends, J. G. Snijders, and Ziegler (2001). *J. Comput. Chem.* **22,** 931-967; b) ADF2016, SCM; Theoretical Chemistry, Vrije Universiteit: Amsterdam, The Netherlands; http://www.scm.com.
43. E. V. Lenthe and E. J. Baerends (2003). *J. Comput. Chem.* **24,** 1142-1156.
44. S. Grimme, S. Ehrlich, and L. Goerigk, (2011). *J. Comp. Chem.* **32**, 1456-1465.
45. S. Sharma, K. K. Chakrahari, J.-Y. Saillard, and C. W. Liu (2018). *Acc. Chem. Res*. **51,** 2475-2483.